^{242}Pu neutron-induced fission cross-section measurement from 1 to 2 MeV neutron energy

P. Marini,[1,2,*] L. Mathieu,[1] M. Aïche,[1] G. Belier,[2] S. Czajkowski,[1] Q. Ducasse,[1] B. Jurado,[1] G. Kessedjian,[3] J. Matarranz,[1] A. Plompen,[4] P. Salvador-Castiñeira,[4,5] J. Taieb,[2] and I. Tsekhanovich[1]

[1]*CENBG, CNRS/IN2P3-Université de Bordeaux 19, Chemin du Solarium, 33175 Gradignan, France*

[2]*CEA, DAM, DIF, F-91297 Arpajon, France*

[3]*LPSC, Université de Grenoble-Alpes, CNRS/IN2P3, LPSC Grenoble - 53, Avenue des Martyrs, 38026 Grenoble, France*

[4]*EC-JRC, Retieseweg 111, 2440 Geel, Belgium*

[5]*National Physical Laboratory, Hampton Road, Teddington TW11 0LW, United Kingdom*

(Received 29 August 2017; published 20 November 2017)

Relative values of the neutron-induced fission cross section $\sigma(n,f)$ of ^{242}Pu have been measured with respect to the standard ^{1}H(n,p) elastic scattering cross section, at average energies of 1.0, 1.4, and 1.9 MeV. The measurements are part of an international effort to reduce uncertainties and provide independent nuclear data relevant for fast-spectrum reactors. The shape of the measured cross section is in good agreement with data from Tovesson *et al.* [Phys. Rev. C **79**, 014613 (2009)] and with the most recent data from Matei *et al.* [Phys. Rev. C **95**, 024606 (2017)], but disagrees with the shapes of ENDF/B-VII.1 and JEFF3.2 evaluations. Absolute values of $\sigma(n,f)$, obtained under some assumptions, indicate an overestimation of $\sigma(n,f)$ in the evaluated libraries at 1.0 and 1.4 MeV, while a good agreement is found with ENDF/B-VII.1 at 1.9 MeV. A careful analysis of the impact of scattered neutrons and anisotropy of the fission fragment angular distribution has been performed. The measurement of the neutron flux by means of a proton-recoil detector is discussed. A comprehensive study of corrections applied to the data, of associated uncertainties, and of correlations between the measurements at the different energies is presented.

DOI: 10.1103/PhysRevC.96.054604

I. INTRODUCTION

Neutron-induced reaction cross sections of actinides between 0.1 and 5 MeV neutron energy are crucial in reactor physics for the development of the next generation nuclear power plants ("Gen IV"). Indeed, four of the six designs under study are based on a fast neutron-energy spectrum. Higher fluxes in the fast region require high precision data in that very region for some minor actinides and structural materials to minimize uncertainties in reactor design parameters. Recent sensitivity studies [1–3] have indicated the desired accuracy of nuclear data necessary to meet the requirements for integral parameters of those systems [1]. Among the highest priorities for a significant reduction of the uncertainties is data on Pu isotopes.

Among these isotopes, ^{242}Pu is produced in nuclear fuel through successive neutron captures and decay processes. In thermal systems, this nonfissile isotope is typically produced faster than it disappears, due to its low thermal fission cross section. In fast reactors, however, a more efficient burning would occur, since the harder fission neutron spectrum better matches its fission threshold. For this isotope, the target accuracy for the fission cross section, $\sigma(n,f)$, is of 5%, to be compared to the current uncertainty of 20%. However, its relatively short half-life implies a high natural activity, which makes the samples difficult to handle, produces a background component in the measurements, and may damage the fission detectors.

Up to the last ten years, most of the data sets for the ^{242}Pu(n,f) cross section available in the Experimental Nuclear Reaction Data Library (EXFOR) [6] dated from the 1970s and earlier. The last decade has seen a renewed interest in this cross section, and experimental efforts have been carried out in Europe and in the United States. Nowadays, numerous data sets exist in the region from the threshold up to 20 MeV [7–15], with a spread which may go up to 10%–15% for energies below 2.5 MeV (see Fig. 1). Quite a large spread is also observed around the resonance-like structure visible at 1.0 to 1.2 MeV present in the evaluated data file and some data sets. The data reported in Ref. [13] by Salvador-Castiñeira *et al.* agree with previous results and evaluations above 1.8 MeV; however, for lower energies, they are well below the evaluations and do not reproduce the resonance-like structure. In contrast, the most recent data by Matei *et al.* [14], obtained by an absolute measurement of neutron fluence with a reference instrument at the National Physical Laboratory, UK, are clearly above the results of Ref. [13] below 1.2 MeV in the resonance-like region, and are consistent within the error bars with ENDF/B-VII.1 [5] and JEFF3.2 [4] evaluations and with data from Tovesson *et al.* [12] and Kogler *et al.* [15] (not available in EXFOR).

In this work we report on new data on ^{242}Pu in the energy range from 1 to 2 MeV, in reference to the neutron-proton ^{1}H(n,p) elastic scattering cross section. This standard is known with a precision around 0.2% over the energy range of this experiment. The chosen energy region covers the beginning of the first-chance fission plateau, i.e., exactly the region which, together with the fission onset, is important for the new generation reactor applications, where the accuracy of the nuclear data needs to be improved and where the most

*paola.marini@cea.fr

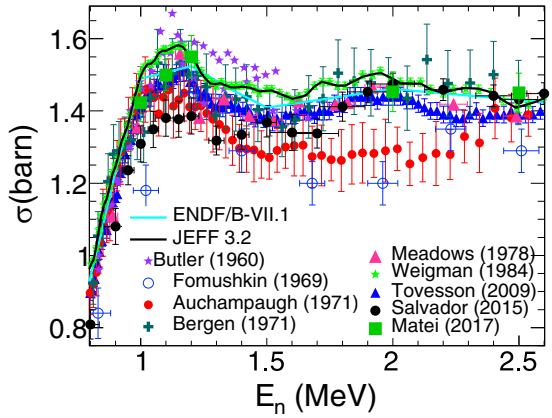

FIG. 1. Main existing data sets (symbols) on ^{242}Pu $\sigma(n,f)$ in the region between 0.8 and 2.6 MeV neutron energy (source EXFOR) and evaluations [4,5] (lines).

recent data disagree. The normalization to the ^{1}H(n,p) elastic scattering cross section in this energy region required a deep study of the limits of applications of the method, as well as the understanding of all the sources of background intrinsic to the method, as detailed in Ref. [16]. These limitations, not known at the time of the experiment, prevented us from accurately extracting the absolute values of the ^{242}Pu $\sigma(n,f)$. Therefore we mainly focus our discussion on the precise determination of the shape of $\sigma(n,f)$.

As the goal of the present work is to attain high precision and carefully evaluate all the sources of uncertainty, the experiment and the data analysis are presented in detail. The paper is organized as follows: Section II describes the neutron source, the target sample and the experimental setup. Section III presents the procedures used to determine the fission cross section, based on the assessment of the fission rate (Sec. III A) and the neutron flux (Sec. III C). In Sec. IV we present the obtained results and discuss the uncertainties and correlations between measurements at different energy settings. Conclusions are given in Sec. V.

II. EXPERIMENTAL SETUP

A. Neutron source

Quasi-monoenergetic neutron beams with energies at zero degree of 1.1, 1.5, and 2.0 MeV were produced in the T$(p,$n$)^{3}$He reaction on a 950 μg/cm^2 TiT solid target at the 4 MV Van de Graaff accelerator of CEA/DIF (France). The solid target had a tritium loading ratio of about 1.53 and was deposited on a Au backing, acting as beam dump and vacuum window. The proton beam intensity was around 4 μA, which gave a neutron flux of about 10^6 $n/($s cm$^2)$ on the target. The average neutron energies impinging on the target are 1.0, 1.4, and 1.9 MeV for the three nominal energies of 1.1, 1.5, and 2.0 MeV, respectively, as discussed in Sec. III E. For the sake of simplicity in the following analysis we will refer to nominal energy values.

Two different beam-dump cooling systems were used for the neutron production target: one based on air, the second one on water. The air-based cooling system was constituted by a thin light-weight pipe, placed few millimeters away from the beam dump, and providing a flux of compressed air on the target. The water-based cooling system was such that a 1 mm thick layer of flowing water was constantly in contact with the backing of the TiT target. The system was equipped with a recirculating water circuit, thus significantly increasing the amount of matter close to the neutron source, compared to the air-based system. Measurements at 1.1 and 1.5 MeV nominal neutron energies were performed with the water-based cooling system, while measurements at 2 MeV nominal neutron energy were done with the air-based one. The measurement at 1.1 MeV was also repeated with the air-based cooling system.

TABLE I. Sample characteristics as provided by the manufacturer.

	^{242}Pu sample
Activity	(0.2472 ± 0.0007) MBq
Thickness	(239.5 ± 2.1) μg/cm^2
Diameter of deposit	(29.95 ± 0.03) mm
Mass	(1.688 ± 0.014) mg
Isotopic purity	99.96518(45)%

B. Target samples

Initially the goal of our experiment was to measure ^{240}Pu and ^{242}Pu $\sigma(n,f)$. Therefore, two 240 μg/cm^2 targets, one of ^{240}Pu and one of ^{242}Pu, were used in this experiment. The samples were prepared by the electrodeposition technique at the EC-JRC target laboratory in Geel [17] and deposited on a 0.25 mm thick Al backing. The diameter of the deposits was 29.95 mm.

The initial activity of the samples was determined by defined solid angle α counting from the manufacturer, with an uncertainty of 0.3% [17]. The α activities were 14.41 and 0.2472 MBq for the ^{240}Pu and ^{242}Pu targets, respectively. As will be discussed in Sec. III A 1, data from the ^{240}Pu target are not exploitable, therefore only the characteristics of the ^{242}Pu target are discussed in the following.

The target mass and the areal density were deduced by the manufacturer from the α activity value [17]. The achieved overall uncertainties were below 1%, and are dominated by the uncertainty on the isotope half-life. The isotopic composition, measured by mass spectrometry, showed that the target isotopic purity was better than 99.9% and the content of fissile contaminants smaller than 0.02%. The characteristics of the ^{242}Pu target are reported in Table I. For similar targets (same diameter and deposition technique) produced at the same time in the same laboratory, an increase of the quantity of matter on the border of about 7%–10% with respect to the center of the deposit was observed by α-particle spectrometry [18]. The analysis procedure performed here takes into account possible inhomogeneities (see Sec. III A 2).

C. Detector setup

The experimental setup is sketched in Fig. 2. It consisted of a fission-fragment detector and a neutron flux detector, placed

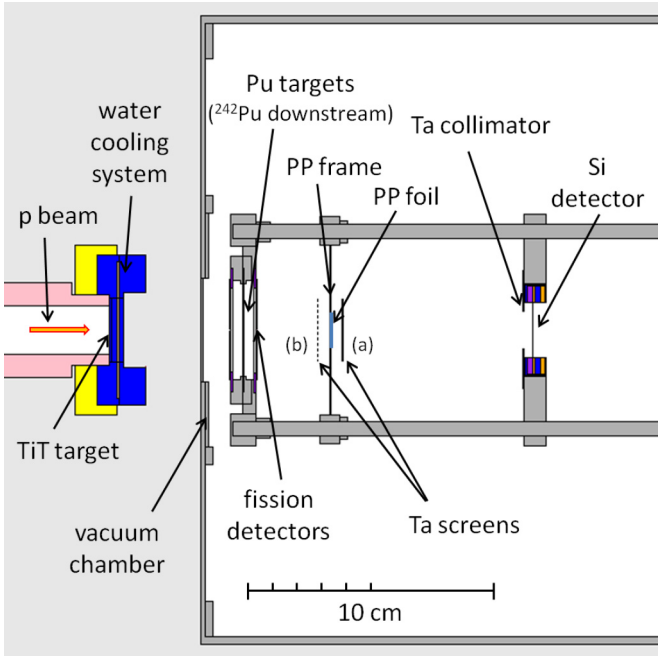

FIG. 2. Experimental setup.

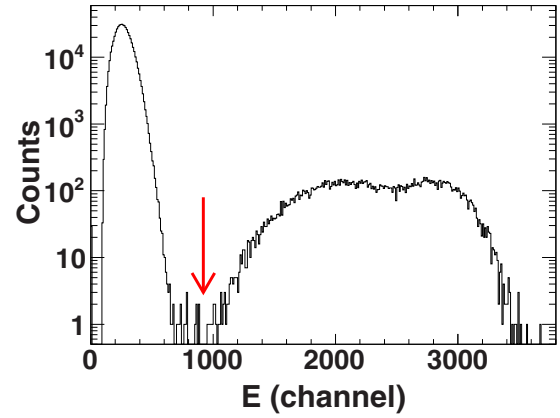

FIG. 3. Experimental pulse-height spectrum for ^{242}Pu spontaneous fission measured with a photovoltaic cell. The energy threshold used to discriminate fission fragments and α background is indicated by the arrow.

in a light-weight aluminum vacuum chamber at 0° with respect to the proton beam axis. The neutron beam was monitored by two detectors (not shown in the figure): a ^{3}He counter, placed at 0°, 3 m from the neutron source, and a BF_3 counter placed at 30° at a distance of 4 m. These detectors were surrounded by a block of paraffin or polyethylene respectively.

1. *Fission detectors*

The two fission targets were placed back to back and encased between two fission-fragment detectors. Photovoltaic cells [19] were chosen for the measurement for their radiation hardness, low sensitivity to α particles, and nonsensitivity to neutrons. Each fission detector was composed of two 40×20 mm^2 solar cells, and separated by a gap of about 0.5 mm. The cells were collimated by their own 34×34 mm^2 support. A complete separation between α background and fission fragments [19,20] could be achieved during the experiment, as shown in Fig. 3, where the double-humped structure of the fission fragment kinetic energy distribution is also visible.

2. *Neutron flux detector*

The neutron flux was measured with a proton-recoil detector, as shown in Fig. 2. The detector consisted of a ^{1}H-rich radiator—a 4 μm polypropylene (PP) foil—mounted on a tantalum (Ta) frame and a 50 μm silicon detector placed downstream the PP. The silicon detector (Si) registered the recoil protons from the ^{1}H(n,p) elastic scattering occurring in the PP foil and emitted into the solid angle defined by a Ta collimator placed in front of the silicon detector. The thickness of the PP foil was chosen to keep the maximum energy lost by the recoil protons below 10% for all the incident neutron energies. The detector system was equipped with a Ta screen, placed downstream the PP foil, to stop the elastic scattered protons, for background measurements (position *a* in Fig. 2). To keep a constant amount of matter in the neutron flux, a Ta screen was placed upstream the PP foil during the standard measurements (position *b*). More details on the technique are given in Sec. III C 2 and the method is extensively described in Ref. [16]. The main characteristics of the proton-recoil detector and the setup are reported in Tables II and III, respectively.

III. ANALYSIS

According to the formalism developed in Refs. [21,22], the fission cross section $\sigma(n,f)(E_n)$ for a given isotope at a neutron energy E_n can be obtained as

$$\sigma(n,f)(E_n) = \frac{R_f}{\Phi_n \frac{\Omega_{\rm Pu}}{\Omega_{\rm PP}} N_{\rm Pu}}(E_n), \qquad (1)$$

where $R_f(E_n)$ is the measured fission rate, $\Phi_n(E_n)$ is the determined incident neutron flux on the PP foil, and $\Omega_{\rm Pu}$ and $\Omega_{\rm PP}$ are the Pu target and PP solid angles, respectively. $N_{\rm Pu}$ is the number of atoms/cm^2 of the ^{242}Pu target.

The fission rate R_f is given by the ratio of the number of neutron-induced fission events, $N_{nf}(E_n)$, in a time Δt, and the

TABLE II. Proton-recoil detector characteristics. Note that the real thickness of the PP foil used in the experiment was not the nominal one (see Sec. III C 1).

Radiator	$(C_3H_6)_n$
Nominal PP thickness	(3.96 ± 0.08) μm
Nominal ^{1}H content	3.23×10^{19} atoms/cm^2
PP density	0.946 g/cm^3
PP collimator diameter	(15.02 ± 0.02) mm
Ta screen diameter	2.5 cm
Ta screen thickness	0.1 mm
Si collimator diameter	(15.02 ± 0.02) mm
Total Si active area	4.0 cm^2
Si thickness	50 μm

TABLE III. Distances between main setup components. The quoted values were measured independently.

	Distance (mm)
neutron source – fission target	54.7 ± 0.5
fission target – photovoltaic cells	5.4 ± 0.2
neutron source – PP	89.7 ± 0.6
PP – silicon detector collimator	78.8 ± 0.2

detector efficiency $\varepsilon_F(E_n)$:

$$R_f(E_n) = \frac{N_{nf}(E_n)}{\varepsilon_f(E_n)\Delta t}, \tag{2}$$

where N_{nf} is the number of fission counts corrected for spontaneous fission.

The neutron flux is obtained as

$$\Phi_n(E_n) = \frac{N_p(E_n)}{\varepsilon_p \overline{\sigma_{el}(n,p)(E_n)} N_H \Delta t}, \tag{3}$$

where N_p is the number of protons scattered in the PP foil and detected in the silicon detector in a time Δt, and $\overline{\sigma_{el}(n,p)}$ is the ^{1}H(n,p) elastic-scattering cross section averaged on the energy spectrum and the scattering angle of neutrons impinging on the PP foil. ε_p is the proton detection efficiency and N_H the number of ^{1}H atoms/cm^2 in the PP foil.

Combining Eqs. (2) and (3), $\sigma(n,f)(E_n)$ can be expressed as

$$\sigma(n,f)(E_n) = \frac{N_{nf}}{N_p}\frac{\varepsilon_p}{\varepsilon_F}\frac{N_H}{N_{\mathrm{Pu}}}\frac{\Omega_{\mathrm{PP}}}{\Omega_{\mathrm{Pu}}}\overline{\sigma_{el}(n,p)}, \tag{4}$$

where the dependence of each term on the mean energy of neutrons impinging on the target, E_n, has been omitted for simplicity. We stress also that the dependence on the measurement time, Δt, cancels in this expression. The determination of each term of Eq. (4), as well as of E_n, is discussed below.

A. Fission rate determination

According to Eq. (2), to determine the fission rate it is necessary to determine the number of neutron-induced fission events, N_{nf}, as well as the fission detection efficiency for each incident neutron energy, $\varepsilon_F(E_n)$.

1. Number of neutron-induced fission events

The first step to determine the number of neutron-induced fission events is the identification of fission fragments and their discrimination from α background.

a. Fission-fragment identification. Fission events were identified by the pulse height delivered by the photovoltaic cells. A typical pulse-height spectrum for ^{242}Pu is shown in Fig. 3. An appropriate threshold was used to separate fission fragments and α background, as shown in the figure. A good α-background–fission-fragment discrimination could be achieved only for ^{242}Pu. Indeed the intense ^{240}Pu α activity (14.4 MBq) severely degraded the detector response during the experiment, despite the radiation hardness of photovoltaic cells. This is shown in Figs. 4(e)–4(h), where the evolution

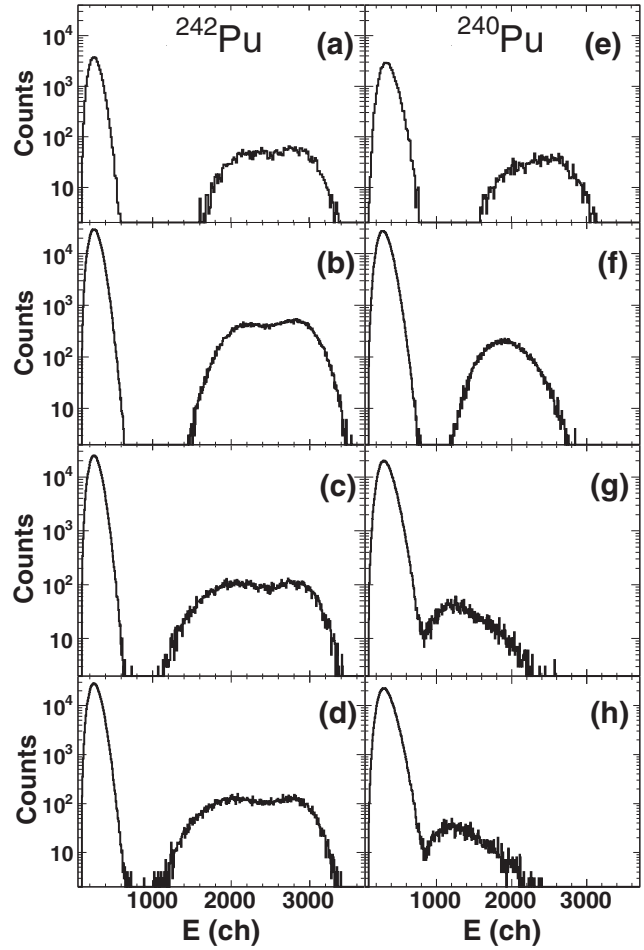

FIG. 4. Fission detector pulse-height spectra for ^{242}Pu (a)–(d) and ^{240}Pu (e)–(h) spontaneous fission at the beginning of the experiment (a),(e) and after 1 (b),(f), 5 (c),(g), and 7 days (d),(h).

over a period of 7 days of the photovoltaic cells pulse-height spectrum is presented. For the ^{242}Pu, the degradation of the detector response was less severe, and the discrimination between α background and fission fragments could be achieved also after seven days of irradiation, as can be seen in Figs. 4(a)–4(d).

The spontaneous-fission rate of the ^{242}Pu sample was determined experimentally by counting when the beam was off. The number of neutron-induced fission events, N_{nf}, was then obtained as

$$N_{nf} = N_{FF} - N_{\mathrm{SF}}, \tag{5}$$

where N_{FF} is the number of detected fission fragments and N_{SF} is the number of spontaneous fissions detected during the measurement and deduced from the spontaneous-fission rate, corrected for the dead time. The statistical uncertainty on the number of detected fission fragments both for spontaneous-fission and neutron-induced events is between 0.5% and 1.5%. The systematic uncertainty on the number of spontaneous-fission fragments N_{SF} is smaller than 0.2%, and is due to the uncertainty of the pulser frequency, which allowed us to measure the run time.

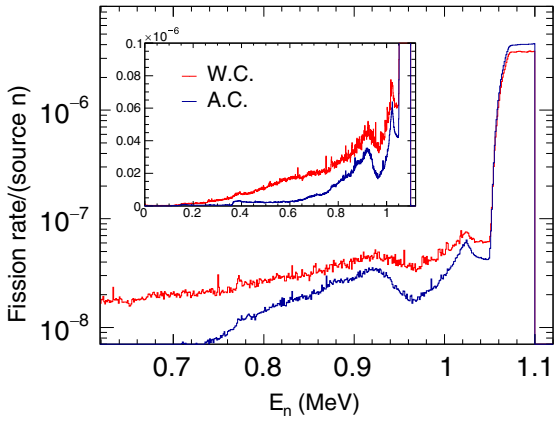

FIG. 5. Simulated fission rate as a function of neutron energy for a 1.1 MeV neutron source. Results for both the water-based (W.C.) and air-based (A.C.) cooling systems are presented. In the MCNP simulation the proton beam energy loss in the TiT target is not implemented.

b. Dead-time correction. The acquisition dead time was taken into account for the determination of the spontaneous-fission rate. We remark that this correction is not necessary for the measurement of the detected fission fragments and of the neutron flux because they were performed simultaneously and on the same Data Acquisition System (DAQ), and should therefore be corrected for the same quantity. The loss of events due to dead time was measured experimentally by a pulse generator signal sent both to the preamplifier of the silicon detector and to a scaler. The correction factor was obtained from the comparison of the number of pulses accepted by the data acquisition system and the total number of sent pulses, and is on the level of 1% with a negligible uncertainty.

c. Scattered neutron correction. The presence of materials in and around the setup introduces an additional component to the neutron flux on the fission target, due to neutron scattering. An example of fission rate as a function of neutron energy is shown in Fig. 5, and was obtained by MCNP [23] simulations. A detailed experimental setup has been implemented and it is sketched in Fig. 6. A peak with a width determined by the angular coverage of the fission target is present, as expected,

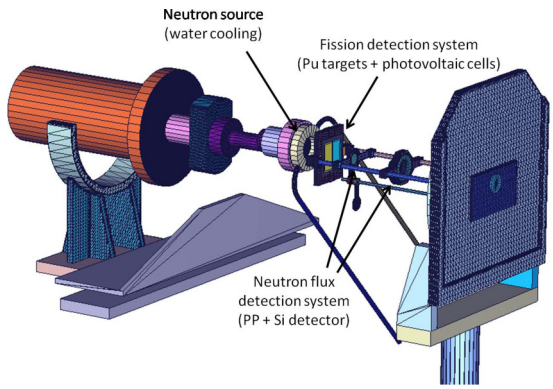

FIG. 6. Experimental setup as modeled in MCNP simulations. Only the back of the vacuum chamber is shown.

TABLE IV. Fraction of ^{242}Pu fission rate (η) due to scattered neutrons for each nominal neutron beam energy and setup configuration, obtained by MCNP simulations.

E_n (MeV)	η	
	Water cooling	Air cooling
1.1	$(12.6 \pm 1.4)\%$	$(6.0 \pm 0.7)\%$
1.5	$(15.9 \pm 1.8)\%$	
2.0		$(6.1 \pm 0.7)\%$

slightly below the nominal neutron beam energy at 0°. A non-negligible rate is also observed for neutron energies well below the neutron beam energy (see inset). Their contribution can be quantified as the integral of the spectrum for energies below the peak (from 0 to 1.05 MeV in Fig. 5, values are reported in Table IV).

The main contribution comes from neutrons scattered on materials close to the neutron production target. As expected, a much higher contribution from the water cooling (W.C.) system is observed (up to 16%) as compared to that from the air cooling (A.C.) system (around 6%). The number of detected fission events must therefore be corrected for this term as

$$N_{nf}(E_n) = N_{nf}^{\mathrm{det}}(1 - \eta(E_n)), \tag{6}$$

where $\eta(E_n)$ is the percentage of fission rate due to scattered neutrons integrated for all the energies from 0 MeV to the lowest limit of the neutron peak. We stress here that η does not account for those scattered neutrons whose energies fall in the neutron peak, since they cannot be disentangled in the simulation from the nonscattered neutrons. The relative uncertainty on this correction is estimated to be around 10% for the geometry (especially for the cooling system), plus about 5% coming from the ingredients of the simulation itself (physics processes, source distribution, cross sections, etc.), to be conservative.

2. *Fission efficiency*

In typical experiments based on ionization chambers (for instance [13,14]), the fission detector efficiency, ε_F, can be easily measured and used to deduce the spontaneous-fission half-life of the isotope of interest. This is not the case for the present setup: the proximity of the fission detector to the target and the target dimensions comparable to those of the cells induce a dependence of the intrinsic efficiency on the target inhomogeneities. The dependence arises from a lower detection probability for fission fragments emitted from the border of the target than for those emitted from the center. Therefore we adopt here the opposite technique, and base the determination of ε_F on the knowledge of the spontaneous-fission half-life. As will be shown, the spontaneous-fission efficiency was used to determine the geometrical and intrinsic efficiencies of the fission detector.

a. Spontaneous-fission efficiency. The measurement of the spontaneous-fission rate from the ^{242}Pu sample gave a precise determination of the spontaneous-fission efficiency of the fission detector, $\varepsilon_{\mathrm{SF}}$, which also accounts for possible target inhomogeneities; see Sec. II B. The $\varepsilon_{\mathrm{SF}}$ measurement

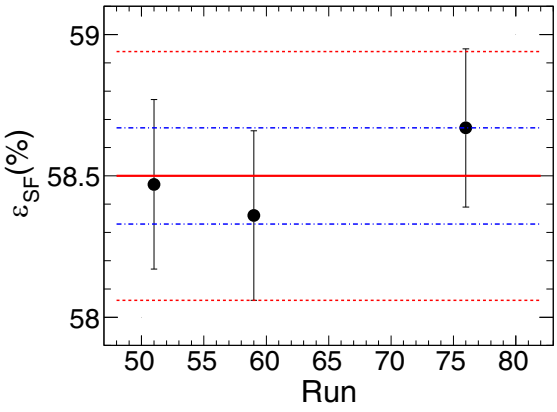

FIG. 7. Spontaneous-fission efficiency with its statistical uncertainty as a function of run number. The full line is the mean value, the blue dashed lines indicate its statistical uncertainty (one standard deviation), the red dotted lines account for both statistical and systematic uncertainties.

was repeated during the experiment to monitor a possible degradation of the detector response due to radiation damage. The obtained efficiency values are plotted in Fig. 7. The overall spontaneous-fission efficiency was measured to be $\varepsilon_{\rm SF} = (58.50 \pm 0.17^{\rm stat} \pm 0.41^{\rm syst})\%$. The systematic uncertainty, which dominates, is mainly due to the uncertainty in the spontaneous-fission branching ratio ($5.51 \times 10^{-6}(4)$, i.e., 0.68% [24]), as the uncertainty in the measurement time is of 0.15%, given by the uncertainty on the pulser frequency used to measure the run-time length.

b. Kinematics and fission-fragment anisotropy effects. The fission detection efficiency at a given neutron energy, $\varepsilon_F(E_n)$, can be obtained as

$$\varepsilon_F(E_n) = \varepsilon_{\rm SF}(1 + \xi(E_n)), \tag{7}$$

where ξ accounts for kinematics effects resulting from the irradiation profile, the moving fissioning system, and the fission-fragment angular anisotropy in the center-of-mass reference system at each incident neutron energy. Monte Carlo simulations accounting for energy and spatial resolutions of the proton beam, energy loss of the proton beam in the tritium target, angular distributions of the neutron beam, and kinematical focusing were performed. Fragment masses, charges, and kinetic energies for the fission of ^{242}Pu at the neutron energy of interest were obtained from the GEF code [25]. The kinematical focusing increases the fission efficiency up to 0.5% of its value with respect to the spontaneous-fission efficiency. The relative uncertainty associated with the correction factor ξ is 10%, and it accounts for the limited knowledge of the setup geometry (distances, dimensions, etc.). The obtained values are reported in Table V.

The anisotropy $W(\theta)/W(90^\circ)$ of the fission fragment angular distribution was then taken into account and parametrized as $\{1 + \alpha \cos^2(\theta)\}$. The values of $W(0^\circ)/W(90^\circ)$ at the nominal incident neutron energy, reported in Table V, were taken from [26] and interpolated for the energy of each simulated incident neutron on the target. This further modifies ε_F by an additional 2.5%, depending on the neutron energy and cannot be neglected in the analysis (see Table V).

The rather flat behavior of ε_F as a function of the incident neutron energy indicates that the increasing kinematical focusing as the neutron energy increases is compensated by the strong effect of the anisotropy. The uncertainty on the anisotropy introduces a relative uncertainty of about 4%–6% on the correction factor ξ, in addition to the uncertainty of 10% (on ξ) from the limited knowledge of the experimental setup. The quoted absolute uncertainties include also the uncertainty on the spontaneous-fission branching ratio, which is dominant.

B. Determination of $N_{\rm Pu}$

The number of atoms in the target, $N_{\rm Pu}$, is obtained from the measured α activity and the half-life, with a total uncertainty of 0.55%, determined by the uncertainty on the half-life for α emission ($3.75 \times 10^5(2)$ y, i.e., 0.53% [27]) and on the deposit area (0.20%).

C. Neutron flux determination

According to Eq. (3), the neutron flux can be calculated from the the amount of ^{1}H atoms/cm^2 present in the PP foil, N_H; the number of protons scattered in the PP foil and detected in the silicon detector, N_p; the ^{1}H(n,p) elastic scattering cross section averaged over the neutron energy spectrum impinging on the PP foil, $\overline{\sigma_{el}(n,p)}$; and the proton detection efficiency, ε_p.

1. Determination of N_H

The thickness of the PP foil as provided by the manufacturer was determined by a weighing technique on a high precision balance. A (71.9 ± 0.6) cm^2 foil was obtained from the same sheet from which the PP foil used during the experiment was cut. This technique relies on the assumption of a homogeneous foil, and does not require knowledge of the material density. The measured number of ^{1}H atoms/cm^2 is $(3.23 \pm 0.07) \times 10^{19}$, assuming a stoichiometry of $(C_3H_6)_n$ without impurities. For a density of 0.946 g/cm^3, it corresponds to a thickness of (3.96 ± 0.08) μm of PP.

TABLE V. Correction factor ξ and fission efficiency ε_F not accounting ($\alpha = 0$) and accounting ($\alpha \neq 0$) for anisotropy.

E_n (MeV)	$\alpha = 0$		$\alpha \neq 0$		
	ξ(%)	ε_F(%)	$1+\alpha$	ξ(%)	ε_F(%)
SF			$\varepsilon_{\rm SF} = (58.50 \pm 0.44)\%$		
1.1	0.25 ± 0.03	58.65 ± 0.46	1.168 ± 0.029	3.09 ± 0.36	60.31 ± 0.50
1.5	0.45 ± 0.05	58.77 ± 0.45	1.141 ± 0.024	2.80 ± 0.31	60.14 ± 0.49
2.0	0.51 ± 0.05	58.80 ± 0.45	1.178 ± 0.020	3.18 ± 0.33	60.36 ± 0.50

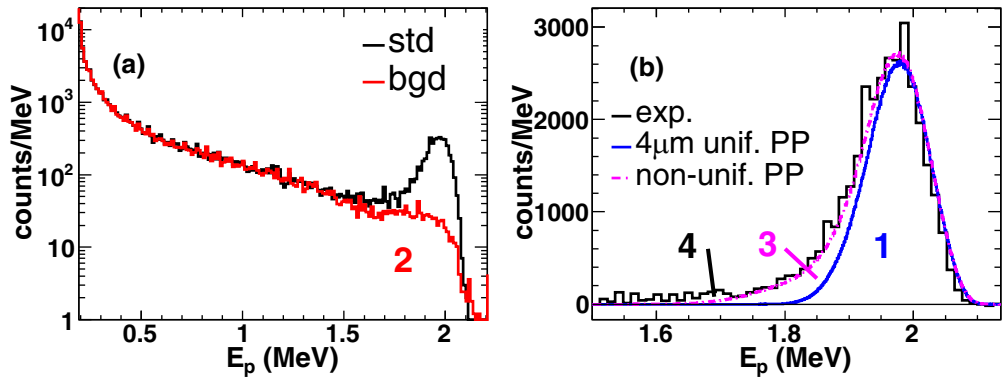

FIG. 8. (a) Proton pulse-height spectra obtained for standard (black) and background (red) measurements at 2 MeV nominal neutron energy. (b) Experimental proton pulse-height spectrum after background subtraction at 2 MeV nominal neutron energy (black), and simulated proton pulse-height spectra for a uniform 4 μm PP foil (blue) and for a non-uniform ^{1}H-contaminated PP foil (pink). Numbers indicate the different contributions to the proton pulse height spectrum (see text).

During the experiment, an oil vacuum pump equipped with filters was used for radioprotection reasons. As shown in Ref. [16], this induces a deposition of hydrogen coming from the oil on the PP foil, which evolves at every opening/pumping and which biases the value of N_H, and consequently the number of detected protons scattered in the PP foil, N_p, up to 20% [16]. It is for this reason that we focus on relative values. Relative values are normalized to the value of theENDF/B-VII.1 cross section at 1.9 MeV (which, we remind the reader, correspond to our measurement at 2 MeV nominal energy). This energy is chosen as reference because of the good agreement between the ENDF/B-VII.1 evaluation and the most recent data sets [5,13,14]. The ^{1}H quantity was therefore determined as the value for which our measured cross section at 1.9 MeV reproduces the ENDF evaluated data. As useful runs were collected on a short time lapse (approximately 4 days) without any additional opening/pumping cycle, in the following we make the assumption that during this period the quantity of ^{1}H did not change significantly. The validity of this assumption is discussed later on in Sec. IV B. The so-determined ^{1}H quantity is therefore used to normalize the cross sections at different energies.

2. *Determination of N_P*

The collimated silicon detector was placed 7.9 cm away from the PP foil (see Table III) and covered 0.44% of the 4π solid angle. Therefore almost only 0° scattered protons, with energies close to the incident neutron beam energy, were detected. These protons produced a peak slightly below the neutron beam energy[1] in the silicon pulse-height spectrum. In the following we refer to this peak as a proton peak. N_p can therefore be determined as the integral of the proton peak. The measured proton pulse-height spectrum is shown in black in Fig. 8(a). To determine N_p it is necessary to identify all the sources of protons, remove or estimate possible background contributions, and establish the limits of integration of the peak.

From a careful analysis, four different components can be identified in the proton pulse-height spectrum. First, there are protons generated in the interaction of direct neutrons impinging on the manufacturer-provided PP foil (1). These are the protons of interest and their number is N_p. In addition, there are contributions from protons generated in the interaction of direct neutrons impinging on ^{1}H-rich or ^{1}H-contaminated materials of the setup (2); direct neutrons impinging on the ^{1}H contamination of the PP foil (3); and scattered neutrons impinging on the PP foil (4). The four contributions are schematically indicated in Fig. 8 and discussed in the following. Note that contributions (3) and (4) are the differences between the 4 μm uniform PP and nonuniform PP spectra, and between the nonuniform PP and the experimental spectra, respectively.

a. Contribution of ^{1}H-rich and/or ^{1}H-contaminated materials of the setup. The contribution (2), which consists of protons generated elsewhere than in the PP foil, can be experimentally measured and subtracted. The recoiling proton spectrum was measured at each energy with two separate measurements, namely, a standard measurement followed by a background measurement. For the latter, a tantalum screen placed between the PP foil and the silicon detector (Ta screen position *a* in Fig. 2) stopped the recoiling protons produced in the PP foil. For a more detailed description of the background correction method and associated corrections we refer the reader to [16].

The proton pulse-height spectra before and after background subtraction, as well as the background spectrum [contribution (2)], are shown in Fig. 8. The ^{3}He neutron monitor was used to normalize the standard and background measurements to the same neutron fluence. The spectrum that results from the background subtraction ["exp." in panel (b)] presents only one peak, corresponding to the protons produced in the interaction of neutrons with the PP foil.

To investigate the remaining two contributions, dedicated Monte Carlo simulations for neutrons and protons passing through the experimental setup were performed. The

[1]This is due to the energy loss of protons in the radiator and to the finite angular opening of the detector.

simulation code takes into account the energy and spatial resolution of the proton beam, energy loss of the proton beam in the tritium target, angular distributions of neutrons, spatial dependence of the (n,p) interactions, energy and angular distribution of the (n,p) elastic scattering cross sections [28], proton energy loss in the PP foil, and energy resolution of the silicon detector, as well as the geometry of the setup.

b. Contribution of scattered neutrons impinging on the PP foil. For kinematic reasons, namely the neutron emission angle and the proton scattering angle, the contribution (4) is significant at energies well below the proton peak energy, and becomes negligible at energies around the proton peak energy. This is illustrated in Fig. 8(b), where the simulated proton pulse-height spectrum obtained for a ^{1}H-contaminated PP foil ("non-unif. PP") is compared to the experimental spectrum. The contribution of scattered neutrons is given by the difference of the two spectra. As this contribution is difficult to evaluate and subtract, it is necessary to limit the range of integration of the proton peak to energies around the proton peak, to minimize the error on N_p.

c. Contribution of direct neutrons impinging on the ^{1}H-contamination of PP the foil. Protons scattered in the manufacturer-provided PP foil or in ^{1}H contamination of PP foil (3) cannot be experimentally distinguished since they both originate by direct neutrons impinging on the foil. Therefore, simulations were run to reproduce the shape of the proton peak, and in particular its asymmetry. It was found that ^{1}H drops of different sizes (up to 16 μm) on the PP foil surface might introduce such asymmetry ["non-unif. PP" in Fig. 8(b)]. This has to be compared to the results obtained for a uniform 4 μm PP foil "[4 μm unif. PP" in Fig. 8(b)].

A common set of parameters describing the contamination of the PP foil (oil droplet sizes) allowed us to obtain a very good agreement of the experimental and simulated proton pulse-height spectra for the three studied incident neutron energies, as shown in Fig. 9. In particular, a good agreement was obtained both for the high energy part of the spectrum, which is determined by the kinematics of protons scattered in the 4 μm regions of the PP foil and the detector energy resolution, and for the low energy part of the spectrum, which is determined by the proton production rate and proton energy loss in the nonuniform regions of the PP foil. We would like to stress that the simulation provides an estimation of the ^{1}H contamination with about 20% precision. Therefore, despite the very good agreement of the spectrum shapes, the number of ^{1}H atoms deduced from the simulation could not be used as a precise and accurate estimation of the real number of ^{1}H atoms. It is therefore necessary to determine N_p for the 4 μm uniform PP foil.

The good agreement between the experimental and simulated ("non-unif. PP") proton spectra supports our understanding of the different contributions to the spectrum, and allowed us to fine tune the simulation for the 4 μm uniform PP foil. The simulation was then normalized to the high energy part of the experimental spectrum. This allowed us to establish a criterion to define the limits of integration of the proton peak, independent of the incident neutron energy. The low energy limit, $E^p_{\rm low}$, was defined as the proton energy for which the number of counts in the 4 μm uniform spectrum is 1/100 of the number of counts at the most probable energy. The high energy limit, $E^p_{\rm high}$, was defined as the maximum detected proton energy. As an example, the used limits of integration are reported in Fig. 9.

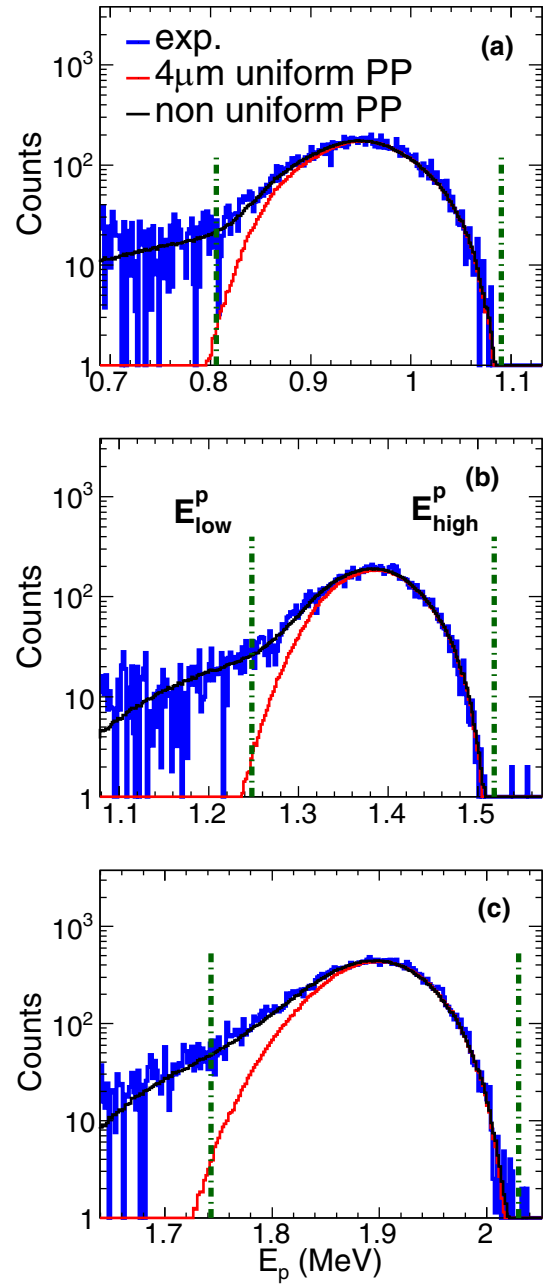

FIG. 9. Comparison of experimental and simulated proton pulse-height spectra for 1.1 (a), 1.5 (b), and 2 MeV (c) nominal neutron energy. The spectra are simulated for a 4 μm uniform and a nonuniform PP foil (see text). The experimental spectra are corrected for the background and represent the whole statistics for each energy. The two vertical lines indicate the energy limits of integration of the proton peak.

The contribution of the ^{1}H contamination to N_p was estimated as the difference between the two simulated proton peak integrals, and the experimental N_p value corresponding

TABLE VI. Mean $\sigma_{el}(n,p)$ and proton detector efficiency ε_p and their absolute uncertainties, as a function of the nominal neutron energy.

E_n (MeV)	$\overline{\sigma_{el}(n,p)}$ (barns)	ε_p(%)
1.1	4.174 ± 0.008	0.885 ± 0.005
1.5	3.475 ± 0.007	0.885 ± 0.005
2.0	2.936 ± 0.006	0.885 ± 0.005

to 4 μm PP thickness was calculated as

$$N_p = N_p^{\text{integral}}(1-p), \tag{8}$$

where N_p^{integral} is the proton peak integral experimentally measured. The obtained values are of 8%, 10%, and 13% for 1.1, 1.5, and 2 MeV nominal neutron energy, respectively. The relative uncertainty on this contribution is estimated at 20%, to be conservative, and arises from the very limited knowledge of the ^{1}H contamination.

The total relative uncertainty on N_p after correction is between 2% and 3%, with a statistical uncertainty between 1% and 1.7%. There are two contributions to the statistical uncertainty. First, there is the statistical uncertainty on the background corrected proton pulse-height spectrum, which contributes to the N_p statistical uncertainty up to 1%. This contribution includes the statistical uncertainty on the standard and background measurements, as well as on the normalization coefficient, used for the background subtraction. Second, there is the uncertainty on E^p_{low} deduced from the simulation, which is evaluated to be 0.01 of the nominal neutron energy, and introduces an uncertainty on N_p between 1% and 1.5%. The systematic uncertainty arises from the 20% relative uncertainty on the correction for the ^{1}H contamination of the PP, which introduces an uncertainty of 1.6%, 2.1%, and 2.7% on N_p for 1.1, 1.5, and 2 MeV nominal neutron energy, respectively.

3. Determination of $\overline{\sigma_{el}(n,p)}$ and ε_p

The aforementioned Monte Carlo simulations (Sec. III C 2) allowed us to estimate the average energy of neutrons impinging on the PP foil for each nominal incident neutron energy, and the corresponding $\overline{\sigma_{el}(n,p)}$, according to the formalism developed in Refs. [21,22]. The obtained values are reported in Table VI. The associated uncertainties arise from a 0.2% systematic uncertainty on $\sigma(n,p)(E_n)$ [28].

Proton detection efficiencies were also determined by simulation. The obtained values are 0.885% for the three neutron energies, with a systematic relative uncertainty of 0.6%. The different contributions to the uncertainty come from the precision on the diameter of the silicon detector collimator (0.26%), on the PP foil diameter (0.05%), and on the measured distances (0.51%) (see Table II). According to kinematics, the proton detection efficiency, ε_p, is independent of neutron energy, provided the differences in the PP irradiation profiles are negligible.

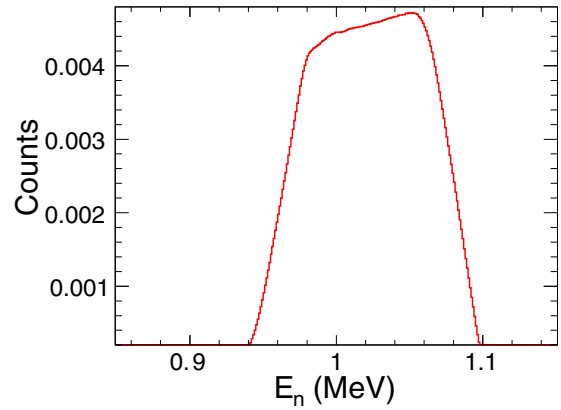

FIG. 10. Energy distributions of neutrons impinging on the ^{242}Pu target for a nominal energy of 1.1 MeV.

D. Determination of the Ω_{Pu}/Ω_{PP} ratio

We would like to stress here that, since the angular distribution of the produced neutrons is not isotropic, Ω_{Pu} and Ω_{PP} of Eq. (1) do not strictly represent the solid angles covered by the detectors, but account also for the mentioned anisotropy, which depends on the neutron energy. The Monte Carlo simulation described in Sec. III C 2 could not be used to determine the ratio Ω_{Pu}/Ω_{PP}, due to the presence of materials between the fission target and the PP. MCNP simulations were therefore performed to account for the neutron transmission. The obtained values of Ω_{PP}/Ω_{Pu} are reported in Table IX. The uncertainties were evaluated to be about 2%, and they arise from the uncertainties on the geometry of the setup, namely 1.6% for the neutron-source–Pu-target distance and 1.3% for the neutron-source–PP-foil distance.

E. Determination of E_n

The simulations described in Sec. III C 2 allowed us to determine the mean energy of neutrons impinging on the Pu target. The energy distribution is shown in Fig. 10 for a nominal 1.1 MeV neutron energy, and do not include scattered neutrons, which have already been accounted for in the fission-rate correction (Sec. III A 1 c). The obtained values are reported in Table IX, where the quoted uncertainties are the root mean squares of the distributions for the different nominal neutron energies. We stress here the relevance of a proper calculation of E_n, which differs up to 7% from the nominal neutron beam energy value. The effect is due to the energy loss of the proton beam in the TiT target and to the angular opening of the fission target ($\theta_{max} = 15^\circ$), and therefore it should be taken into account when working with thick production targets and/or with a large fission target placed close to the neutron source.

Unfortunately, it is not clear to us whether the calculation of the average neutron energy has been performed for the data reported by Salvador-Castiñeira *et al.* [13] and Matei *et al.* [14], to which our results will be compared in the following.

IV. RESULTS

The neutron-induced fission cross section values of ^{242}Pu from this experiment are reported in Table IX and plotted in

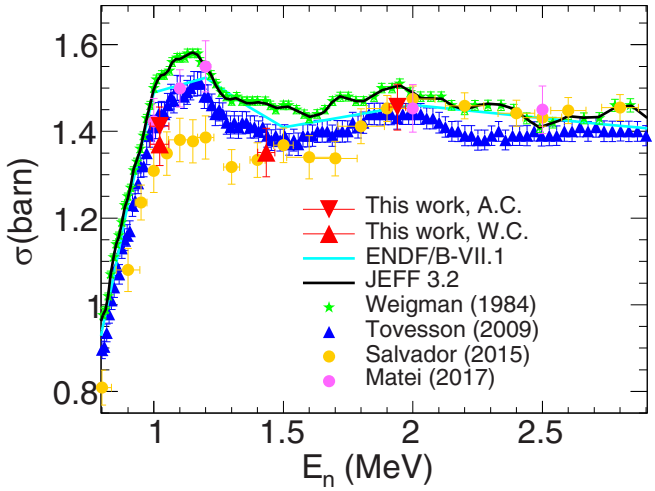

FIG. 11. Comparison of the results of this experiment obtained with the air-based (red triangles) and water-based (red inverted triangles) cooling systems to the evaluations [4,5] and the most relevant experiments. Our results are normalized to the ENDF-B/VII.1 $\sigma(n,f)$ value at 1.9 MeV.

Fig. 11 with experimental data from earlier works and nuclear evaluated data from ENDF-B/VII.1 [5] and JEFF-3.2 [4] libraries. We remind the reader that data were normalized to the ENDF-B/VII.1 evaluation at 1.9 MeV (which corresponds to our measurement at 2 MeV nominal energy). An attempt is also made to extract the absolute cross section values, under some assumptions that are discussed in detail.

In the following we first discuss the uncertainties and covariances among data, and then we compare our results to the existing data.

A. Uncertainty calculations and covariances

The statistical relative uncertainty of the presented data ranges from 1.0% to 1.7%, and does not represent the main contribution to the final uncertainty. The systematic uncertainty ranges from 2.8% to 3.8% for the relative $\sigma(n,f)$ values and from 3.6% to 4.5% for the absolute values. There are three main contributions to the systematic uncertainty. The first is the uncertainty on the solid angles ratio, Ω_{PP}/Ω_{Pu}, which arises from the uncertainty on the measured distances. This contribution could be reduced by using a bigger setup, which implies a reduced statistics if the measurement time is kept constant. The second contribution is the uncertainty affecting the number of fission events, N_{nf}, which mainly comes from the correction to account for the scattered neutrons inducing fission. Because of the significance of this latter correction for the measurements with the water cooling system, and the difficulties to precisely measure the distances due to the amount of matter present in the setup, the uncertainties for the 1.1 MeV (W.C.) and 1.5 MeV neutron energies are larger. This indicates the need to further reduce the amount of matter possibly interacting with neutrons in and around the experimental setup. The last contribution is the uncertainty affecting the number of detected protons, N_p, which mainly comes from the correction to account for the ^{1}H-rich impurities deposited on the PP foil. This contribution could be reduced by paying special care to the handling of the foil and using a dry vacuum pump during the experiment. An additional contribution is present in the systematic uncertainty for the absolute values, which arises from the uncertainty on N_H of 2.0%. This points to the need to further improve the whole PP weighing procedure.

TABLE VII. Correlation matrix among the measurements at different energies of relative $\sigma(n,f)$ values for air-based (labeled as A.C.) and water-based (labeled as W.C.) cooling systems.

	1.1 (W.C.)	1.5 (W.C.)	2.0 (A.C.)	1.1 (A.C.)
1.1 (W.C.)	1	0.63	0.44	0.67
1.5 (W.C.)	0.63	1	0.38	0.41
2.0 (A.C.)	0.44	0.38	1	0.54
1.1 (A.C.)	0.67	0.41	0.54	1

The correlation between two measurements at different neutron energies, E_i and E_j, was estimated to be [20,22,29]

$$\mathrm{cor}(\sigma(E_i),\sigma(E_j)) = \sqrt{\frac{\mathrm{Var}^{\mathrm{sys}}(E_i)\mathrm{Var}^{\mathrm{sys}}(E_j)}{\mathrm{Var}(E_i)\ \mathrm{Var}(E_j)}}, \qquad (9)$$

where $\mathrm{Var}(E_i)$ and $\mathrm{Var}^{\mathrm{sys}}(E_i)$ are the total and shared systematic variances associated with the measurement at the energy E_i, respectively.

The obtained values for the relative and absolute $\sigma(n,f)$ results are reported in Tables VII and VIII, respectively, for the different incident neutron energies and cooling systems. The highest correlation is obtained between measurements realized with the same cooling system. This is due to the fact that they share the same set of distances, and the correction to the fission rate for scattered neutrons is obtained by implementing in the simulation the same geometry for the neutron source region. The correlations among absolute values of $\sigma(n,f)$ are higher than those for relative values. This is due to the systematic uncertainty on N_H, which is common to all the absolute measurements for the different energies.

B. Relative values of ^{242}Pu $\sigma(n,f)$

As mentioned, the present relative $\sigma(n,f)$ values were normalized to the ENDF-B/VII.1 $\sigma(n,f)$ value at 1.9 MeV. This energy is chosen as reference because of a good agreement between evaluations and the most recent data sets [5,13,14].

The statistical uncertainties affecting the data are about three times smaller than the systematic uncertainties. Moreover

TABLE VIII. Correlation matrix among the measurements at different energies of absolute $\sigma(n,f)$ values for air-based (labeled as A.C.) and water-based (labeled as W.C.) cooling systems.

	1.1 (W.C.)	1.5 (W.C.)	2.0 (A.C.)	1.1 (A.C.)
1.1 (W.C.)	1	0.73	0.60	0.78
1.5 (W.C.)	0.73	1	0.54	0.58
2.0 (A.C.)	0.60	0.54	1	0.69
1.1 (A.C.)	0.78	0.58	0.69	1

the data are rather correlated (between 0.4 and 0.7; see Table VII). This indicates that, independently of the chosen normalization, the measured shape of $\sigma(n,f)$ is reliable.

For the 1.0 MeV average neutron energy, the results obtained with both the water and air cooling systems are presented. Although the result obtained with the water cooling system is lower than the one obtained with the air cooling system, they are consistent within the error bars. Indeed, the difference between the two measurements is 3.0%, and the sum of the statistical and uncorrelated systematic uncertainties of the two measurements is 2.3% and 2.8%, for the A.C. and W.C. cases, respectively. The agreement found between these two measurements has two important consequences. First, as discussed in Sec. III C 1, in the analysis we have assumed that the quantity of ^{1}H contamination deposited on the PP foil did not vary during the measurement. This assumption is supported by the observed agreement between the two measurements, which were performed once at the beginning (W.C.) and once at the end (A.C.) of the experiment. Second, such agreement validates the MCNP calculations on the contribution of parasitic fission to N_{nf}, which goes up to 15% for the water cooling system (see Sec. III A 1 c). In addition, the similar shape of the two experimental proton pulse-height spectra measured for this energy (not shown here) rules out the possibility of a compensation of errors from the two mentioned effects.

The measured shape of $\sigma(n,f)$ is in agreement with neither the ENDF-B/VII.1 nor the JEFF-3.2 trends. Indeed, our data are at least 4.5% lower than the ENDF-B/VII.1 evaluated data at 1.0 and 1.4 MeV average energy. This difference is larger than the total uncertainties at both energies. Similar conclusions can be drawn when normalizing and comparing our data to JEFF-3.2 evaluation.

When comparing our results to existing data, a general good agreement is found with Tovesson's values for the three neutron energies. Moreover, at 1.4 MeV average neutron energy our result is in agreement with the value reported by Salvador-Castiñeira. This indicates that the slope of the $\sigma(n,f)$ between 1.4 and 1.9 MeV is steeper than the one given by the evaluations. Unfortunately no data from Matei exist at this neutron energy.

At 1.0 MeV average energy, our results are in pretty good agreement both with Matei's and Tovesson's data. A worse agreement is found with data from Salvador-Castiñeira, which are, however, within the error bars. Around this energy, both Matei and Tovesson observe a resonance-like structure, which is less pronounced in Salvador-Castiñeira's results. Our results neither confirms nor INVALIDATE the presence of a marked resonance: additional measurements at higher energies, between 1.1 and 1.2 MeV, would be necessary to determine its amplitude.

C. Absolute values of ^{242}Pu $\sigma(n,f)$

As previously discussed, a ^{1}H contamination of the PP foil during the experiment prevented us from extracting absolute cross section values. However, they can be determined under two hypothesis. First, the PP foil provided by the manufacturer has a uniform thickness. This assumption is supported by the observations reported in Ref. [16], where it was shown that consistent results could be obtained using different PP foils cut from the same PP sheet. The number of ^{1}H atoms in the PP foil was therefore determined as described in Sec. III C 1 for a manufacturer-provided PP foil. The second assumption is that the absolute values of the correction to N_p discussed in Sec. III C 2 c are correct for the three studied neutron energies.

The absolute $\sigma(n,f)$ values obtained under these assumptions are reported in Table IX. A very good agreement is observed between the absolute values and the relative values normalized to the ENDF-B/VII.1 1.9 MeV $\sigma(n,f)$ value. The difference between the two data sets is smaller than 0.4% for all the measured neutron energies. Therefore, while a good agreement with the ENDF-B/VII.1 evaluation at 1.9 MeV is confirmed, both the ENDF-B/VII.1 and JEFF-3.2 values overestimate the $\sigma(n,f)$ at 1.0 and 1.4 MeV average energies.

V. CONCLUSIONS

Relative values of the ^{242}Pu neutron-induced fission cross section were measured at 1.0, 1.4, and 1.9 MeV average energies with respect to the standard ^{1}H(n,p) elastic scattering cross section, with the aim of providing independent measurements. Two cooling systems were used during the experiment for the neutron source.

The neutron fluence was measured with a proton-recoil detector. ^{1}H pollution of the setup prevented the estimation of the quantity of ^{1}H present in the radiator of the proton-recoil detector. Therefore, the presented cross section values were normalized to the ENDF-B/VII.1 value at 1.9 MeV. Absolute values of $\sigma(n,f)$ were also determined, although under some assumptions.

The impact of scattered neutrons and anisotropy of the fission fragment angular distribution was carefully investigated by simulations and accounted for in the final results. For the present setup, scattered neutrons increase the fission rate of up to 16%, making the correction crucial to obtain accurate results, and indicating the need to reduce as much as possible the amount of matter close to the neutron source. Given the compact geometry of the fission target and fission detector, the anisotropy of the fission fragment angular distribution significantly modifies the fission detection efficiency. These effects should be generally accounted for in cross section measurements with similar setups.

In the recoil-proton based measurement of the neutron flux, the contribution of protons scattered from the ^{1}H contamination of the PP foil was evaluated and corrected for. To be conservative, the uncertainties on each correction factor deduced by simulation were evaluated to be between 10% and 20%. Special attention was dedicated to the evaluation of the effective energy of neutrons impinging on the fission target, which turned out to be significantly lower than the nominal neutron energy.

A careful analysis of all the sources of uncertainty was performed. The uncertainties on the final cross section values are below 5%, as requested by the Nuclear Energy Agency. The statistical uncertainty is below 1.7% for all the neutron energies. The systematic uncertainty is below 3.8% and 4.5% for relative and absolute $\sigma(n,f)$ values, respectively.

TABLE IX. Different terms of Eq. (4) for each nominal neutron energy E_n. Relative $\sigma(n,f)$ values normalized to the ENDF-B/VII.1 $\sigma(n,f)$ value at 1.9 MeV (seventh column) and absolute $\sigma(n,f)$ values (eighth column; see text).

E_n (MeV)	N_{nf}/N_p	$\varepsilon_P/\varepsilon_F$	Ω_{PP}/Ω_{Pu}	$\overline{\sigma_{el}(n,p)}$ (barns)	$\overline{E_n}$ (MeV)	$\sigma(n,f)$ (barns)	$\sigma_{abs}(n,f)$ (barns)
1.1 (W.C.)	$3.922 \pm 1.2\%^{stat}$ $\pm 2.3\%^{sys}$	0.01465 $\pm 1.0\%$	0.1066 $\pm 2.4\%$	4.174 $\pm 0.2\%$	1.024 ± 0.036	$1.373 \pm 1.2\%^{stat}$ $\pm 3.3\%^{sys}$	$1.375 \pm 1.2\%^{stat}$ $\pm 4.1\%^{sys}$
1.5 (W.C.)	$4.583 \pm 1.7\%^{stat}$ $\pm 3.0\%^{sys}$	0.01472 $\pm 1.0\%$	0.1075 $\pm 2.4\%$	3.475 $\pm 0.2\%$	1.434 ± 0.033	$1.354 \pm 1.7\%^{stat}$ $\pm 3.8\%^{sys}$	$1.355 \pm 1.7\%^{stat}$ $\pm 4.5\%^{sys}$
2.0 (A.C.)	$6.100 \pm 1.0\%^{stat}$ $\pm 2.8\%^{sys}$	0.01466 $\pm 1.0\%$	0.1033 $\pm 2.1\%$	2.936 $\pm 0.2\%$	1.940 ± 0.032	$1.457 \pm 1.0\%^{stat}$ $\pm 3.5\%^{sys}$	$1.459 \pm 1.0\%^{stat}$ $\pm 4.2\%^{sys}$
1.1 (A.C.)	$4.244 \pm 1.3\%^{stat}$ $\pm 1.8\%^{sys}$	0.01466 $\pm 1.0\%$	0.1014 $\pm 2.1\%$	4.174 $\pm 0.2\%$	1.022 ± 0.036	$1.414 \pm 1.3\%^{stat}$ $\pm 2.8\%^{sys}$	$1.415 \pm 1.3\%^{stat}$ $\pm 3.6\%^{sys}$

Correlations between the measurements at different energies are presented and are the highest for measurements performed with the same cooling system. Also, absolute cross section values are more correlated than relative cross section data.

The data are in very good agreement with the recent measurements from Tovesson *et al.* [12] and Matei *et al.* [14], and in agreement with data from Salvador-Castiñeira *et al.* [13] above 1.0 MeV. The measured shape of $\sigma(n,f)$ is not in agreement with the JEFF3.2 andENDF/B-VII.1 libraries, while a very good agreement of the absolute value at 1.9 MeV is found with ENDF/B-VII.1. This indicates an overestimation of the evaluations between 1 and 1.4 MeV, also supported by the measured absolute values for these energies.

ACKNOWLEDGMENTS

We wish to acknowledge the support of G. Sibbens from the target laboratory EC-JRC for providing Pu targets. This work was supported by the European Commission within the EURATOM FP7 framework program through ANDES (Contract FP7-249671).

[1] NEA Nuclear Data High Priority Request List, http://www.nea.fr/html/dbdata/hprl

[2] OECD/NEA Working Party on Evaluation and Co-operation (WPEC) Subgroup 26 Final Report, http://www.nea.fr/html/science/wpec/volume26/volume26.pdf

[3] Report of the numerical results from the evaluation of the nuclear data sensitivities: Priority list and table of required accuracies for nuclear data, edited by E. Gonzalez-Romero, Deliverable D5.11 from IP-EUROTRANS (unpublished).

[4] OECD/NEA, JEFF3.2 Evaluated data Library - Neutron Data. technical report (unpublished).

[5] M. B. Chadwick, M. Herman, P. Obložinský, M. E. Dunn, Y. Danon, A. C. Kahler, D. L. Smith, B. Pritychenko, G. Arbanas, R. Arcilla, R. Brewer, D. A. Brown, R. Capote, A. D. Carlson, Y. S. Cho, H. Derrien, K. Guber, G. M. Hale, S. Hoblit, S. Holloway, T. D. Johnson, T. Kawano, B. C. Kiedrowski, H. Kim, S. Kunieda, N. M. Larson, L. Leal, J. P. Lestone, R. C. Little, E. A. McCutchan, R. E. MacFarlane, M. MacInnes, C. M. Mattoon, R. D. McKnight, S. F. Mughabghab, G. P. A. Nobre, G. Palmiotti, A. Palumbo, M. T. Pigni, V. G. Pronyaev, R. O. Sayer, A. A. Sonzogni, N. C. Summers, P. Talou, I. J. Thompson, A. Trkov, R. L. Vogt, S. C. van der Marck, A. Wallner, M. C. White, D. Wiarda, and P. G. Young, Nucl. Data Sheets **112**, 2887 (2011), special issue on ENDF/B-VII.1 Library.

[6] N. Otuka, E. Dupont, V. Semkova, B. Pritychenko, A. I. Blokhin, M. Aikawa, S. Babykina, M. Bossant, G. Chen, S. Dunaeva, R. A. Forrest, T. Fukahori, N. Furutachi, S. Ganesan, Z. Ge, O. O. Gritzay, M. Herman, S. Hlavac, K. Kato, B. Lalremruata, Y. O. Lee, A. Makinaga, K. Matsumoto, M. Mikhaylyukova, G. Pikulina, V. G. Pronyaev, A. Saxena, O. Schwerer, S. P. Simakov, N. Soppera, R. Suzuki, S. Takacs, X. Tao, S. Taova, F. Tarkanyi, V. V. Varlamov, J. Wang, S. C. Yang, V. Zerkin, and Y. Zhuang, Nucl. Data Sheets **120**, 272 (2014).

[7] G. F. Auchampaugh, J. A. Farrell, and D. W. Bergen, Nucl. Phys. A **171**, 31 (1971).

[8] D. W. Bergen and R. R. Fullwood, Nucl. Phys. A **163**, 577 (1971).

[9] J. W. Meadows, Nucl. Sci. Eng. **85**, 271 (1983).

[10] H. Weigmann, J. A. Wartena, and C. Bürkholz, Nucl. Phys. A **438**, 333 (1985).

[11] P. Staples and K. Morley, Nucl. Sci. Eng. **129**, 149 (1998).

[12] F. Tovesson, T. S. Hill, M. Mocko, J. D. Baker, and C. A. McGrath, Phys. Rev. C **79**, 014613 (2009).

[13] P. Salvador-Castiñeira, T. Bryś, R. Eykens, F.-J. Hambsch, A. Göök, A. Moens, S. Oberstedt, G. Sibbens, D. Vanleeuw, M. Vidali, and C. Pretel, Phys. Rev. C **92**, 044606 (2015).

[14] C. Matei, F. Belloni, J. Heyse, A. J. M. Plompen, and D. J. Thomas, Phys. Rev. C **95**, 024606 (2017).

[15] T. Kogler, R. Beyer, A. R. Junghans, R. Massarczyk, R. Schwengner, and A. Wagner, Phys. Procedia **64**, 150 (2015).

[16] P. Marini, L. Mathieu, L. Acosta, M. Aïche, S. Czajkowski, B. Jurado, and I. Tsekhanovich, Nucl. Instrum. Methods Phys. Res., Sect. A **841**, 56 (2017).

[17] G. Sibbens, A. Moens, R. Eykens, D. Vanleeuw, F. Kehoe, H. Kühn, R. Wynants, J. Heyse, A. Plompen, R. Jakopič, S. Richter, and Y. Aregbe, J. Radioanal. Nucl. Chem. **299**, 1093 (2014).

[18] P. Salvador-Castineira, Ph.D. thesis, Universitat Politecnica de Catalunya, 2014 (unpublished).

[19] G. Siegert, Nucl. Instrum. Methods **164**, 437 (1979).
[20] G. Kessedjian, G. Barreau, M. Aïche, B. Jurado, A. Bidaud, S. Czajkowski, D. Dassié, B. Haas, L. Mathieu, L. Tassan-Got, J. N. Wilson, F. J. Hambsch, S. Oberstedt, I. Al Mahamid, J. Floyd, W. Lukens, and D. Shuh, Phys. Rev. C **85**, 044613 (2012).
[21] C. Grosjean, Ph.D. thesis (in French), Université de Bordeaux I, 2005 (unpublished).
[22] G. Kessedjian, Ph.D. thesis (in French), University of Bordeaux, 2008 (unpublished).
[23] D. B. Pelowitz *et al.*, MCNPX 2.7 E Extensions, Los Alamos National Laboratory, Report No. LA-UR-10-00481, 2010 (unpublished).
[24] G. Belier (private communication).
[25] K.-H. Schmidt, B. Jurado, C. Amouroux, and C. Schmitt, Nucl. Data Sheets **131**, 107 (2016).
[26] J. E. Simmons, R. B. Perkins, and R. L. Henkel, Phys. Rev. **137**, B809 (1965).
[27] M. R. Bhat, in *Evaluated Nuclear Structure Data File ENSDF, Nuclear Data for Science and Technology* (Springer-Verlag, Berlin, 1992).
[28] J. C. Hopkins and G. Breit, Nucl. Data Tables A **9**, 137 (1971).
[29] Q. Ducasse, Ph.D. thesis (in French), Université de Bordeaux, 2015 (unpublished), hal.in2p3.fr/tel-01262725